MOLECULAR AND CELLULAR BIOLOGY, Dec. 2005, p. 11131–11144 Vol. 25, No. 24
0270-7306/05/$08.00+0 doi:10.1128/MCB.25.24.11131–11144.2005

periostin Null Mice Exhibit Dwarfism, Incisor Enamel Defects, and an Early-Onset Periodontal Disease-Like Phenotype

Hector Rios,[2]# Shrinagesh V. Koushik,[1]# Haiyan Wang,[1]# Jian Wang,[1] Hong-Ming Zhou,[1] Andrew Lindsley,[1] Rhonda Rogers,[1] Zhi Chen,[2] Manabu Maeda,[1,3] Agnieszka Kruzynska-Frejtag,[4] Jian Q. Feng,[2] and Simon J. Conway[1]*

Cardiovascular Development Group, Herman B. Wells Center for Pediatric Research, Indiana University School of Medicine, Indianapolis, Indiana 46202[1]; Department of Oral Biology, School of Dentistry, University of Missouri—Kansas City, Kansas City, Missouri 64108[2]; Nara Medical University, Kashihara City, Nara 634-8521, Japan[3]; and Wroclaw Medical University, 50-367 Wrocław, Poland[4]

Received 25 August 2005/Returned for modification 21 September 2005/Accepted 23 September 2005

Periostin was originally identified as an osteoblast-specific factor and is highly expressed in the embryonic periosteum, cardiac valves, placenta, and periodontal ligament as well as in many adult cancerous tissues. To investigate its role during development, we generated mice that lack the *periostin* gene and replaced the translation start site and first exon with a *lacZ* reporter gene. Surprisingly, although *periostin* is widely expressed in many developing organs, *periostin*-deficient (*peri*^{lacZ}) embryos are grossly normal. Postnatally, however, ~14% of the nulls die before weaning and all of the remaining *peri*^{lacZ} nulls are severely growth retarded. Skeletal analysis revealed that trabecular bone in adult homozygous skeletons was sparse, but overall bone growth was unaffected. Furthermore, by 3 months, the nulls develop an early-onset periodontal disease-like phenotype. Unexpectedly, these mice also show a severe incisor enamel defect, although there is no apparent change in ameloblast differentiation. Significantly, placing the *peri*^{lacZ} nulls on a soft diet that alleviated mechanical strain on the periodontal ligament resulted in a partial rescue of both the enamel and periodontal disease-like phenotypes. Combined, these data suggest that a healthy periodontal ligament is required for normal amelogenesis and that periostin is critically required for maintenance of the integrity of the periodontal ligament in response to mechanical stresses.

Periostin is a secreted cell adhesion protein of relatively unknown function that has homology with the insect growth cone guidance protein fasciclin I (14, 28). Periostin is thought to function as a homophilic adhesion molecule during bone formation and can support osteoblastic cell line attachment and spreading (10). Purified recombinant periostin has been shown to be a ligand for αvβ3 and αvβ5 integrins promoting integrin-dependent cell adhesion and motility (8). Multiple reports have also demonstrated elevated periostin levels in neuroblastoma (25), in epithelial ovarian cancer (8), and in non-small-cell lung carcinoma (25) that had undergone epithelial-mesenchymal transformation and metastasized. Moreover, it has been shown that periostin potently promotes metastatic growth of colon cancer by augmenting cell survival via the Akt/protein kinase B pathway (1). Periostin is also associated with extracellular matrix (ECM) deposition following myocardial infarction (27) and may be a factor responsible for ventricular dilation (11).

The purpose of this study was to determine if *periostin* is critical for mouse development and to address what role it may play in the wide spectrum of tissues and pathological processes that have been linked to its expression. We also sought to clarify if the developmentally suggestive spatiotemporal regulation of periostin expression is actually required for tooth and heart morphogenesis. We have previously shown that periostin is a useful marker of mesenchymal cells that have undergone epithelial-mesenchymal transformation in the developing heart and is expressed in areas that divide the primitive heart tube into a four-chamber heart (15, 17). Additionally, periostin expression remains in the adult valves (15). Furthermore, we demonstrated that periostin is expressed in the developing teeth at the sites of epithelial-mesenchymal interaction and suggested that periostin could play multiple roles as a primary responder molecule during tooth development and may be linked to deposition and organization of other ECM adhesion molecules during maintenance of the adult tooth, particularly at the sites of hard-soft tissue interface (14). Here we describe the generation and characterization of *periostin* null mice with a *lacZ* reporter gene (*peri*^{lacZ}). Rather unexpectedly, given its intriguing developmental expression, *peri*^{lacZ} nulls are viable in utero and appear grossly normal at birth, suggesting that periostin may not be critical for early mouse development. However, there is a postnatal requirement for periostin, as there are defects in the adult periosteum, cartilage, cardiac valves, and periodontal ligament (PDL)—tissues that normally express periostin throughout adulthood. In this paper, we address the postnatal role of periostin and show that it is vital for maintenance of PDL structure and function during postnatal development.

MATERIALS AND METHODS

Gene targeting. To generate *peri*^{lacZ} knock-in mice, we screened a 129SvJ mouse embryonic stem (ES) cell genomic DNA library (Genome System Inc., St. Louis, MO) by PCR and identified a bacterial artificial chromosome (BAC) clone that contains the genomic DNA that codes for the *periostin* gene. BAC DNA was isolated using a large-construct purification kit (QIAGEN Inc., Valencia, CA), and Southern blots were used to confirm the identity and integrity of the clone. A replacement-targeting vector was constructed where the bacterial

* Corresponding author. Mailing address: Riley Hospital for Children, 1044 West Walnut Street, Room R4 W379, Indiana University School of Medicine, Indianapolis, IN 46202. Phone: (317) 278-8780. Fax: (317) 278-5413. E-mail: siconway@iupui.edu.
# These authors contributed equally.

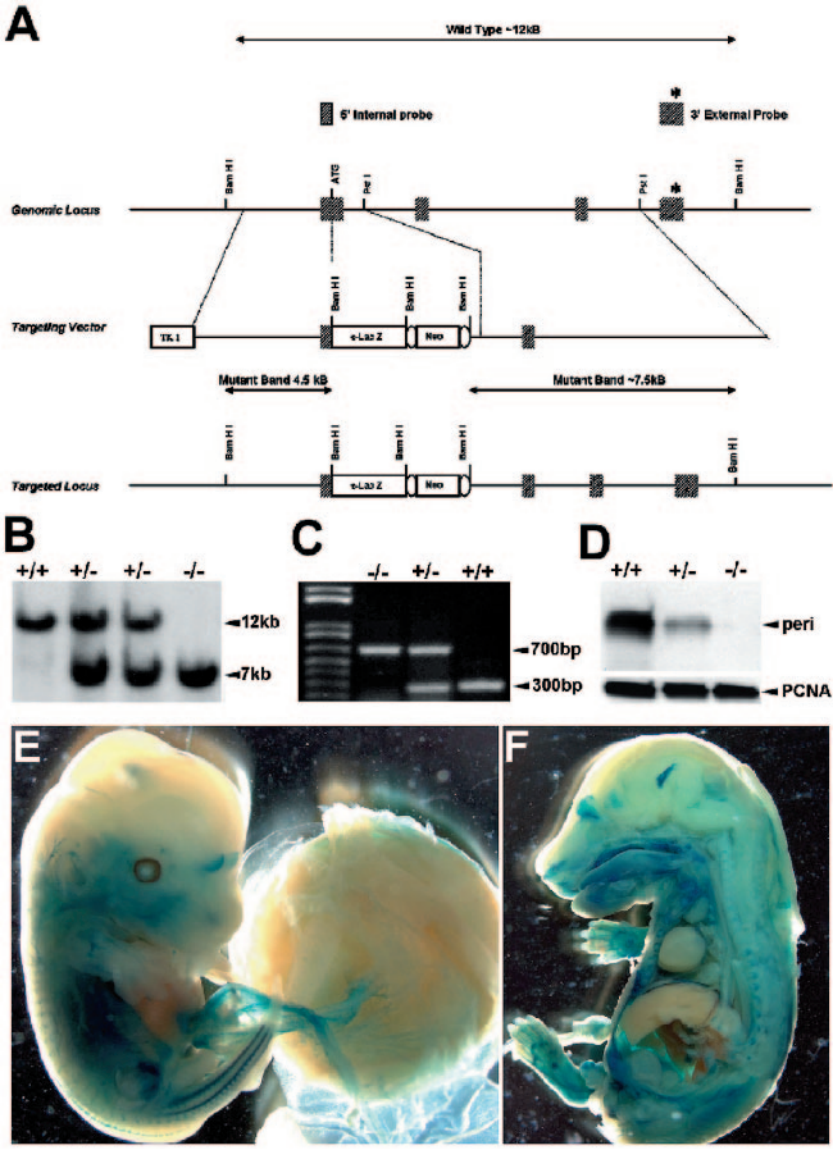

FIG. 1. Construction of the targeting vector and generation of *peri*^{lacZ} knock-in mice. (A) The targeted mouse locus (top line) flanking exons 1, 2, and 3 are shown. A promoterless *IRES-lacZ-neo-loxP* cassette was inserted into exon 1 in the targeting construct (middle line), and the resulting targeted allele is shown (bottom line). TK, thymidine kinase. Both Southern blotting (B) and PCR genotyping (C) were used to identify the correctly targeted ES clones and to genotype the +/+, +/−, and *peri*^{lacZ} null mice. (D) Western blot analysis of periostin protein revealed that there is a complete absence of periostin expression in the newborn nulls and that the heterozygous mutants express only ~30 to 50% of the normal levels of periostin protein. (E and F) Whole-embryo staining of *lacZ* expression in E14 heterozygous and E16 *peri*^{lacZ} null mice. Note widespread expression, particularly within the peripheral nervous system, craniofacial region, dermis of the skin, and body cavities. However, *lacZ* expression is absent in the fetal liver and restrictively expressed in the central nervous system, as staining is only within the olfactory lobe and the choroid plexus (F).

β-galactosidase gene was knocked into the *periostin* gene locus. The 5′ homology arm, a 3.9-kb DNA fragment that contains all the 5′ untranscribed region and promoter elements, was PCR amplified using a high-fidelity Thermal Ace DNA polymerase kit (Invitrogen, Inc., Carlsbad, CA). Primers used were as follows: sense (5′ GCgtcgacCTAAGGTGGACAGTGCGGAAGAC-3′) and antisense (CctcgagCTTCAGCCCTGAGCTCCGTCC-3′). In the PCR, these primers were engineered to produce a 5′ SalI site (in lowercase letters) and a 3′ XhoI site (in lowercase letters), which enabled us to directionally clone the insert in frame with a promoterless *IRES-lacZ-neo-loxP* cassette (13). The resultant vector expressed the *lacZ* reporter under the control of the *periostin* promoter. A 5.3-kb PstI 3′ homology arm was cloned in frame into the 3′ end of the floxed *IRES-lacZ-neo-loxP* cassette. This resulted in a targeting vector where the translation start site and all of the first exon and ~300 bp of the first intron were deleted (Fig. 1A). The complete targeting construct was cloned into the thymidine kinase-negative selection vector (13). Genomic DNA was isolated from 88 ES clones that survived positive-negative selection using previously established protocols (13). Southern hybridization on BamHI-digested DNA was used for both primary and secondary screening. Targeting was confirmed by a 214-bp 3′ external probe (Fig. 1B) and a 400-bp 5′ internal probe. The 3′ external probe (exon 4) was used as the primary screen where the wild-type allele (12 kb) can be easily distinguished from the targeted allele (7.5 kb). The blots were then stripped and reprobed using the 5′ internal probe, which gives a wild-type allele (12 kb) that could be easily distinguished from the targeted allele (4.5 kb). Seven correctly targeted ES clones were identified, and three were used to generate chimeras using standard protocols. Chimeras were subsequently bred with C57BL/6 mice, and tail DNA analyzed by Southern blotting was used to identify

periostin heterozygotes. These were subsequently interbred to generate homozygotes within the C57BL/6 background.

Mouse breeding. Mice were weaned at 3 weeks of age and were then fed distilled water and either NIH-31 complete mouse diet pellets or powdered Teklad LM-485 complete mouse diet (both contain the same ingredients and crude protein, fat, and fiber contents; Harlan). Mice were maintained under specific-pathogen-free conditions with a cycle of 12 h of light and 12 h of dark. The animal use protocols were approved by the Institutional Animal Care and Use Committee at IUPUI (study no. 2707).

PCR genotyping. Genotyping was determined by PCR analysis (Fig. 1C) of genomic DNA with primers p01 (5′-AGTGTGCAGATGTTTGCTTG-3′) and p02 (5′-ACGAAATACAGTTTGGTAATCC-3′) to detect the wild-type allele (~300 bp) and primers p01 (5′-AGTGTGCAGATGTTTGCTTG-3′) and p03 (5′-CAGCGCATCGCCTTCTATCG-3′ to detect the targeted allele (~700 bp).

Reverse transcription-PCR. cDNA was synthesized from RNA isolated from +/+, +/−, and *peri*^{lacZ} null embryonic day 13 (E13), newborn, and adult pooled tissues (n = 6 individuals per sample) using a Superscript-II kit (Invitrogen) with 5 μg RNA and oligo(dT) primer. Dilutions of cDNA (1:30 to 1:100) were amplified with specific periostin primers and normalized with GAPDH (glyceraldehyde-3-phosphate dehydrogenase) as described previously (4, 15).

Western blotting of tissue extracts. PCR-genotyped mouse embryonic, newborn, and adult tissues were isolated and microdissected in cold phosphate-buffered saline (pH 7.4), and protein was isolated as described previously (14). Samples were normalized using a monoclonal anti-proliferating cell nuclear antigen antibody (DAKO) at a 1:10,000 dilution, and the relative levels of periostin were measured by use of our affinity-purified antiperiostin rabbit polyclonal antibody at a 1:10,000 dilution as described previously (14).

***lacZ* and skeletal analysis.** Tissue isolation, fixation, and processing for *lacZ* staining was carried out as described previously (13) and was done similarly for skeletal Alcian blue/Alizarin red staining (15).

Preparation of histological sections. Heads, limbs, and ribs from +/+ and *peri*^{lacZ} null mice were dissected and fixed in 4% paraformaldehyde at 4°C overnight and processed for paraffin sectioning (6 μm). Embryonic and fetal samples were then dehydrated, embedded in paraffin, and sectioned at a thickness of 6 μm for hematoxylin and eosin (H&E) staining according to standard procedures (9, 14). Adult samples were initially demineralized in a 10% EDTA solution (Sigma, St. Louis MO) over 3 weeks and then dehydrated, embedded in paraffin, and sectioned. Safranin-O staining was used to visualize proteoglycans (31).

Immunohistochemistry. Immunostaining of periostin (1:6,000 dilution), α-smooth muscle actin (αSMA) (1:5,000 dilution; Sigma, St. Louis, MO), collagen types I and III (1:1,000 dilution for each; a gift from Larry Fisher, NIH/NIDCR), MF20 (Developmental Studies Hybridoma Bank, University of Iowa, Iowa City), enamelin, ameloblastin, and amelogenin (1:2,000 dilution; a gift from Jan Hu, University of Michigan) was performed on paraffin sections as previously described (14). Immunological reactions were visualized by use of a Vector ABC kit and a peroxidase-diaminobenzidine reaction. Sections were counterstained with hematoxylin and mounted on glass slides. Negative controls were obtained by substituting the primary antibody with serum. For tartrate-resistant acid phosphatase (TRAP) staining, a commercial kit (Sigma, St. Louis, MO) was used according to the manufacturer's instructions. TRAP activity was detected by use of naphthol AS-TR phosphate containing 10 mM L-(+)-tartaric acid as the substrate. These sections were also counterstained with hematoxylin.

Fertility of female *peri*^{lacZ} null mice. Eight- to 12-week-old female +/+, heterozygous, and *peri*^{lacZ} null mice (n = 10 for each genotype) were subjected to a continuous mating study. Two female mice were housed with one 10-week-old male mouse that was known to be fertile, and male mice were rotated weekly. Cages were monitored daily, and the numbers of pups and litters were recorded. Superovulation was induced in 3-week-old immature +/+ and *peri*^{lacZ} null females. Essentially, mice were injected with single intraperitoneal injections of 5 units of pregnant mare serum gonadotropin (Sigma) for 48 h followed by injections of 5 units of human chorionic gonadotropin (Sigma) for a further 18 h. Ovaries and oviducts were harvested and analyzed histologically as described above.

Backscatter scanning electron microscopy (BSEM). Specimens from wild-type and *peri*^{lacZ} null littermates at ages from 1 day to 5 months were fixed as described above, washed, and dehydrated. After dehydration, the specimens were attached to a stub and sputtered with gold/palladium. The gold/palladium-coated specimens were examined by use of a FEI/Philips XL30 field emission environmental scanning electron microscope (SEM). For the cross-sectional analysis after dehydration in ascending concentrations of ethanol, the teeth were fractured under a dissecting microscope and mounted on aluminum stubs with the fractured surface facing upward, sputter coated with Au-Pd, and examined with a field emission SEM.

TEM. Transmission electron microscopy (TEM) sample isolation, fixation, and processing were carried out as previously described (13). Briefly, tissues were examined using a Philips CM12 scanning TEM (STEM). For tissues, bone specimens were fixed with 4% paraformaldehyde and 2% glutaraldehyde solution buffered at pH 7.4 with 0.1 M sodium cacodylate for 8 h at room temperature. The specimens were then washed and dehydrated in an ethanol series, embedded in Polybed 812 resin (Polyscience, Warrington, PA), polymerized for 72 h at 60°C, thin sectioned with a Sorvall MT 5000 ultramicrotome (Sorvall, Norwalk, CT), and mounted on copper grids. The sections were stained with uranyl acetate and lead citrate and viewed with a FEI-Philips SM12 STEM (Hillsboro, OR).

Measurement of postnatal growth parameters and histomorphometry. Sequential measurements of weight and body dimensions were made every 2 weeks, and detailed long bone and rib measurements were made following skeletal Alcian blue/Alizarin red staining (5) by use of AxioVision4 Interactive Measurement Wizard software with a StemiSV11 Apo Zeiss dissecting microscope. Histomorphometric analysis was carried out by choosing 10 to 15 fields in +/+ and *peri*^{lacZ} null metaphyses of femurs.

Statistical analysis. All data are presented as means ± standard deviations of the mean. Student's t test was applied for data comparison, and P values were assigned, with 0.05 or 0.01 being significant.

RESULTS AND DISCUSSION

Generation of *peri*^{lacZ} knock-in mice. The *periostin* gene was disrupted by homologous recombination using the strategy described above to generate +/− *peri*^{lacZ} mice (Fig. 1). These mice were indistinguishable from +/+ littermates in gross appearance, fecundity, weight gain, and histological organ surveys into advanced ages. Heterozygote intercrosses and timed pregnancies produced embryos (E9 to 18.0) with roughly Mendelian ratios of +/+ (n = 96), +/− (n = 206), and −/− (n = 87) offspring (n = 50 litters). Furthermore, newborn +/+ (n = 101), +/− (n = 197), and −/− (n = 82) offspring were also born at similar ratios with an average litter size of 6.9 (n = 55 litters). This deletion removed the DNA encoding the translation start site and all of the first exon and ~300 bp of the first intron of the *periostin* sequence, replacing it with the bacterial β-galactosidase reporter gene. Thus, homozygous embryos carrying two copies of this *lacZ-neo* cassette are null for the *periostin* gene. Reverse transcription-PCR analysis of mRNA prepared from E13 embryos and newborns showed a ~50% reduction in *periostin* expression in the heterozygotes and a complete absence in the *peri*^{lacZ} nulls (data not shown). This absence was confirmed by Western blotting for newborns (Fig. 1D) and immunohistochemistry for adult heads and E14 placentas (Fig. 2), demonstrating that periostin protein is undetectable in mutants and there is a ~50 to 70% decrease in protein levels in heterozygotes (Fig. 1D). Furthermore, as neither Western nor immunohistochemical analysis detected any secreted periostin protein within either the null placentas or embryos, maternal-to-fetal transfer of periostin does not occur. As there is no apparent compensatory increase in periostin levels produced from the normal allele in heterozygous mice and since they are indistinguishable from their wild-type littermates, the ~50 to 70% reduction in protein does not appear significant enough to cause obvious defects.

Null pups appear grossly normal. Newborns or 1-week-old pups homozygous for the absence of *periostin* could not be distinguished visually from wild-type littermates by gross appearance (Fig. 3A), size, or weight (n = 29; 2-day-old +/+ mice were 3.34 ± 0.10 g [$P < 0.005$], and *peri*^{lacZ} nulls were 3.2 ± 0.15 g [$P < 0.005$] [using a two-tailed Student t test and unequal variance analysis]). Examination of the patterns of

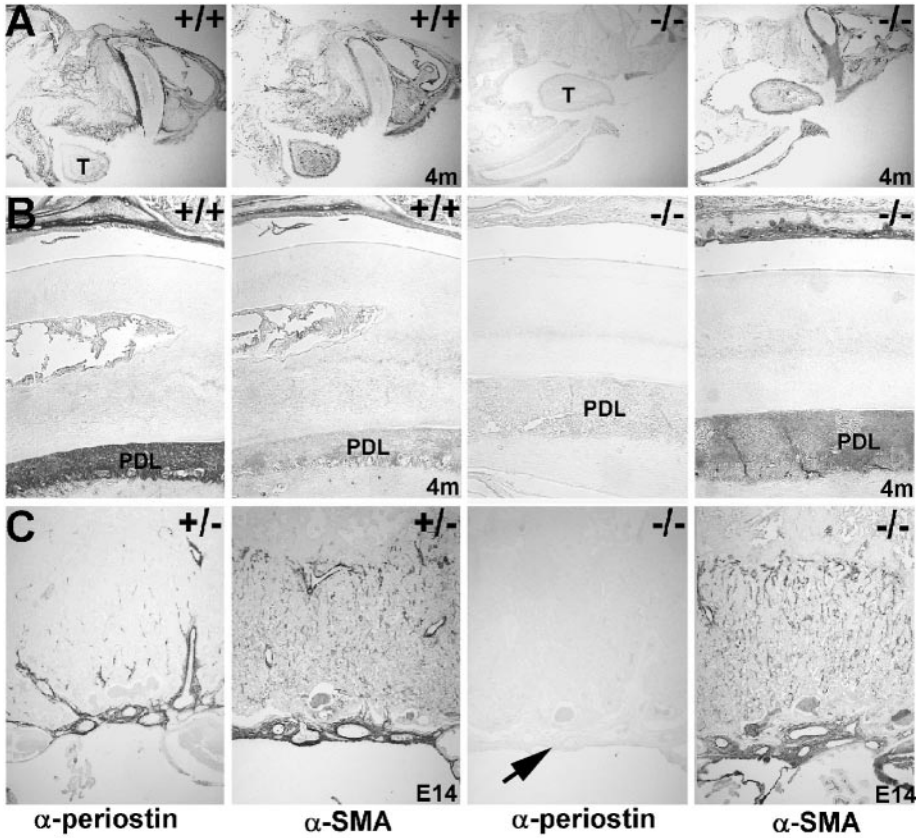

FIG. 2. Immunohistochemical analysis of periostin expression in null mice. (A and B) Periostin protein is highly expressed within the 4-month-old wild-type craniofacial structures (A), particularly in the PDL as well as around the skull and in the periosteum. Note that while periostin is highly expressed in the wild-type PDL (B) but barely detectable in the tongue ("T" in panel A), αSMA is expressed only weakly in PDL but is highly expressed in the tongue. However, there is no detectable periostin protein present throughout the entire *peri*^{lacZ} null head, but αSMA (a positive control to ensure that the protein was intact) is normally expressed. (C) Since periostin protein can be secreted, the patterns of expression in the E14 placenta were analyzed. While periostin protein is confined to the normal fetal heart, embryonically derived umbilical cord, chorionic plate, and larger blood vessels in the labyrinthine part of the placenta, αSMA is highly expressed through all the smooth muscle cells of the labyrinthine part of the control (+/−) and *peri*^{lacZ} null fetal placentas. However, periostin protein is absent from the null placenta (arrow), even though the mother is heterozygous and expresses secreted periostin.

peri^{lacZ} reporter gene expression (Fig. 1E and F) revealed that they were also indistinguishable between the heterozygous and null mice in utero and that they recapitulated the patterns for endogenous mRNA expression (4, 17). Furthermore, histopathologic examination of cardiac valves, teeth, umbilical vessels, placenta, and periosteum around the skeletal elements (the major in utero sites of *periostin* expression) did not reveal any morphological abnormalities (data not shown). We also used both Alizarin red/Alcian blue bone/cartilage staining (Fig. 1C) and radiography (Fig. 3A) to analyze the knockout skeleton, as the outer bone surface is covered by the fibrocellular periostin-expressing periosteum containing osteoblasts, osteoclasts, and other bone deposition/resorption/maintenance factors. However, neither technique revealed any differences (absences, malformations, or extra elements) in the null newborns. The fact that the numbers of skeletal elements and their arrangement have not changed indicates that the absence of periostin from the periosteum/osteoblasts does not alter the early determinants of the pattern formation process but rather may be involved in subsequent growth, maturation, and maintenance and/or repair of individual elements. The lack of any in utero phenotypes despite the robust expression in the embryonic and fetal periosteum, cardiac valves, placenta, and periodontal ligament tissues is somewhat surprising and suggests either that *periostin* is not required in utero or that the role of *periostin* is compensated for by another gene. Indeed, there is another closely related secreted fasciclin-containing adhesion molecule in mammals called transforming growth factor-induced clone H3 (βigH3). Furthermore, both genes are induced by transforming growth factor signaling and are coexpressed in a number of embryonic tissues (6, 17), although their postnatal expression patterns are more divergent. Further studies will be needed to address potential genetic compensation and/or possible interaction of these two *fasciclin*-containing adhesion genes.

Postnatal lethality in some *peri*^{lacZ} null mice. Although heterozygote intercrosses gave rise to newborn litters with roughly normal Mendelian ratios, ~14% of the nulls died within 2 to 3 weeks of birth. Genotyping of 4- to 6-month-old litters (n = 194 litters) revealed there were fewer *peri*^{lacZ} nulls (n = 239) than +/+ mice (n = 325) or +/− mice (n = 638) and that 40 −/− mice (n = 24 male and 16 female) had died, indicating

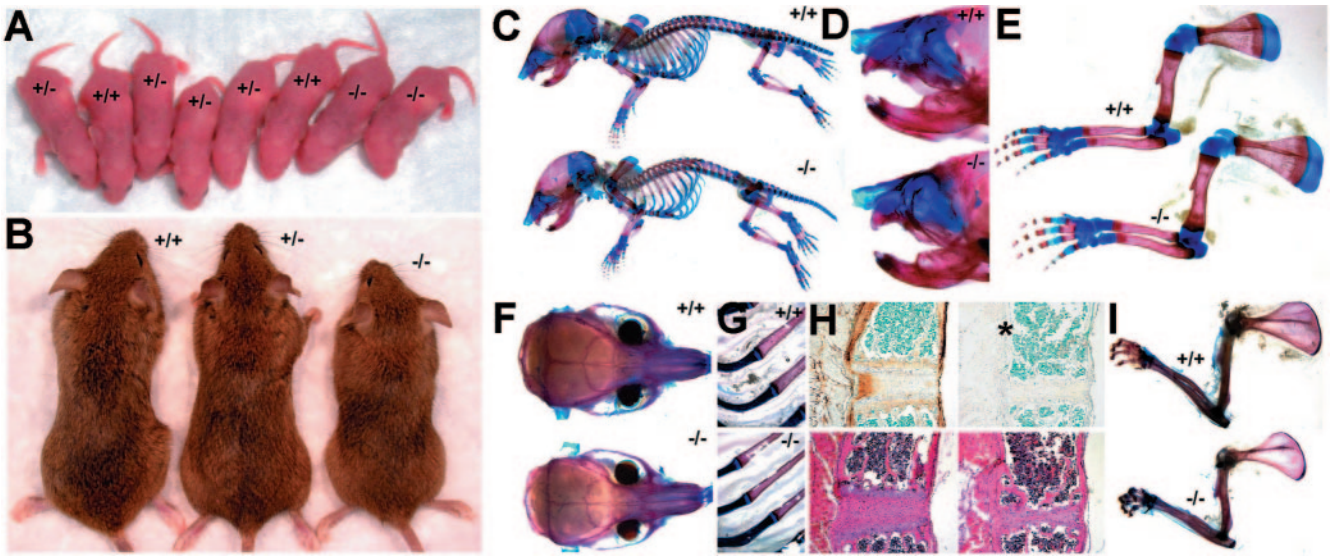

FIG. 3. *peri*^{lacZ} knockout postnatal growth retardation and skeletal defects. Newborn (A) and adult (B) mice. Note that all three genotypes are indistinguishable among the 1-day-old mice ($n = 55$ litters) but that the 4-month-old adult *peri*^{lacZ} null mice are significantly smaller (~15 to 30%) and weigh less (~50%) than their wild-type (+/+) and heterozygous (+/−) littermates ($n = 29$ litters). (C to I) Alizarin red/Alcian blue staining of the skeleton of +/+ and null (−/−) newborns (C to E) and 4-month-old adults (F to H) after skin removal. (C) Lateral view of intact newborns; note that the nulls are identical in size and structure to their normal littermates. Close-ups of the craniofacial region (D) and forelimbs (E); note that there are no differences in lengths and diameters between newborn genotypes. (F) Coronal comparison of the adult skulls; note that the null skulls are ~7% shorter and ~15% narrower than those of +/+ mice ($n = 7$ +/+ and 9 −/− male mice). Similarly, Alizarin red/Alcian blue staining of +/+ and null adult ribs (G) and sternums (H) illustrates skeletal anomalies within the nulls. Note that the null ribs are ~22% narrower in diameter and 12% shorter in length and that periostin expression is absent from the periosteum (indicated by ∗) around the null sternum. Additionally, H&E staining revealed that the adult null cartilaginous sternal growth plates were reduced in area and that there were fewer trabeculae present than in normal littermates. In contrast to what was observed with newborns, adult forelimbs (I) from *peri*^{lacZ} nulls are undersized relative to those from littermates, as null scapular (~23%), humerus (~16%), ulna (~11%), and radius (~11%) are all reduced in length ($n = 7$ +/+ and 9 −/− male mice).

periostin is required postnatally. Given our previous demonstration of robust *periostin* expression throughout valvulogenesis and in the adult heart (15), we analyzed the nonviable preweaning *peri*^{lacZ} hearts. Large acellular deposits of ECM that resulted in discontinuities in the valves were present in the valve leaflets, and there were ectopic islands of αSMA-positive cells present in null leaflets (data not shown; detailed characterization of cardiovascular anomalies in follow-up paper). Given the size and position of these deposits and the inappropriate smooth muscle cells, it is likely that valvular insufficiency is the cause of perinatal lethality in this subpopulation of *peri*^{lacZ} null mice.

Postnatal growth defects of *peri*^{lacZ} null mice. Growth retardation was detectable 3 to 4 weeks after birth, and *peri*^{lacZ} adult mice were consistently smaller than +/− and +/+ littermates (Fig. 3B). The decline in null growth rates occurred around weaning, and dwarfism remained throughout the life of mice. On average, both the male and female adult nulls weighed ~50% less ($n = 20$; 12-week-old +/+ males were 33.7 ± 0.23 g [$P < 0.005$] and females were 27.5 ± 0.36 g [$P < 0.005$], while *peri*^{lacZ} null males were 16.8 ± 0.31 g [$P < 0.005$] and *peri*^{lacZ} null females were 14.57 ± 0.39 g [$P < 0.005$] by a two-tailed Student *t* test and unequal variance analysis) and were ~15 to 30% smaller by morphometric analysis (Fig. 3). Coronal comparison of the adult skulls demonstrated that the adult null skulls are ~7% shorter and ~15% narrower than those of its +/+ littermates ($n = 7$ +/+ and 9 −/− male 4-month-old mice). When undersized ribs and forelimbs from *peri*^{lacZ} nulls were compared to those from +/+ littermates, it was found that the *peri*^{lacZ} null ribs are ~22% narrower in diameter and ~12% shorter in length, while the null scapular (~23%), humerus (~16%), ulna (~11%), and radius (~11%) are also all reduced in length ($n = 7$ +/+ and 9 −/− male 4-month-old mice). Histological examination of adult null ribs (Fig. 3G) revealed that the cartilaginous growth plates were reduced in area and that there were fewer trabeculae present than in normal littermates. Similarly, adult null limbs (Fig. 4B, lower panels) also exhibited reductions in the cancellous bony trabeculae network. Significantly, periostin protein is highly expressed both in the outer periosteum, which gives rise to the bone collar covering all skeletal elements, including cancellous bone, and within the inner endosteal osteoblasts that secrete the vascularized bone-specific matrix (Fig. 4A). Detailed analysis of the skeletal preparations also revealed that in contrast to the newborns, 100% of the 4-month-old male and female *peri*^{lacZ} null alveolar bone adjacent to the incisors showed signs of abnormal remodeling, which was subsequently confirmed by radiography. This further highlighted a postnatal requirement for *periostin* gene function.

As zebra fish periostin is required for the adhesion of muscle fiber bundles to the myoseptum (analogous to the mammalian tendon) and for the differentiation of muscle fibers (16), and given the dwarfism/skeletal dysplasia, we used histology and TEM to assess the periosteum and adhesion of muscle fiber bundles to bones and adjoining muscles. Both revealed that the periosteum is present and intact around the null bones and, unlike what is found for zebra fish, mouse periostin is not

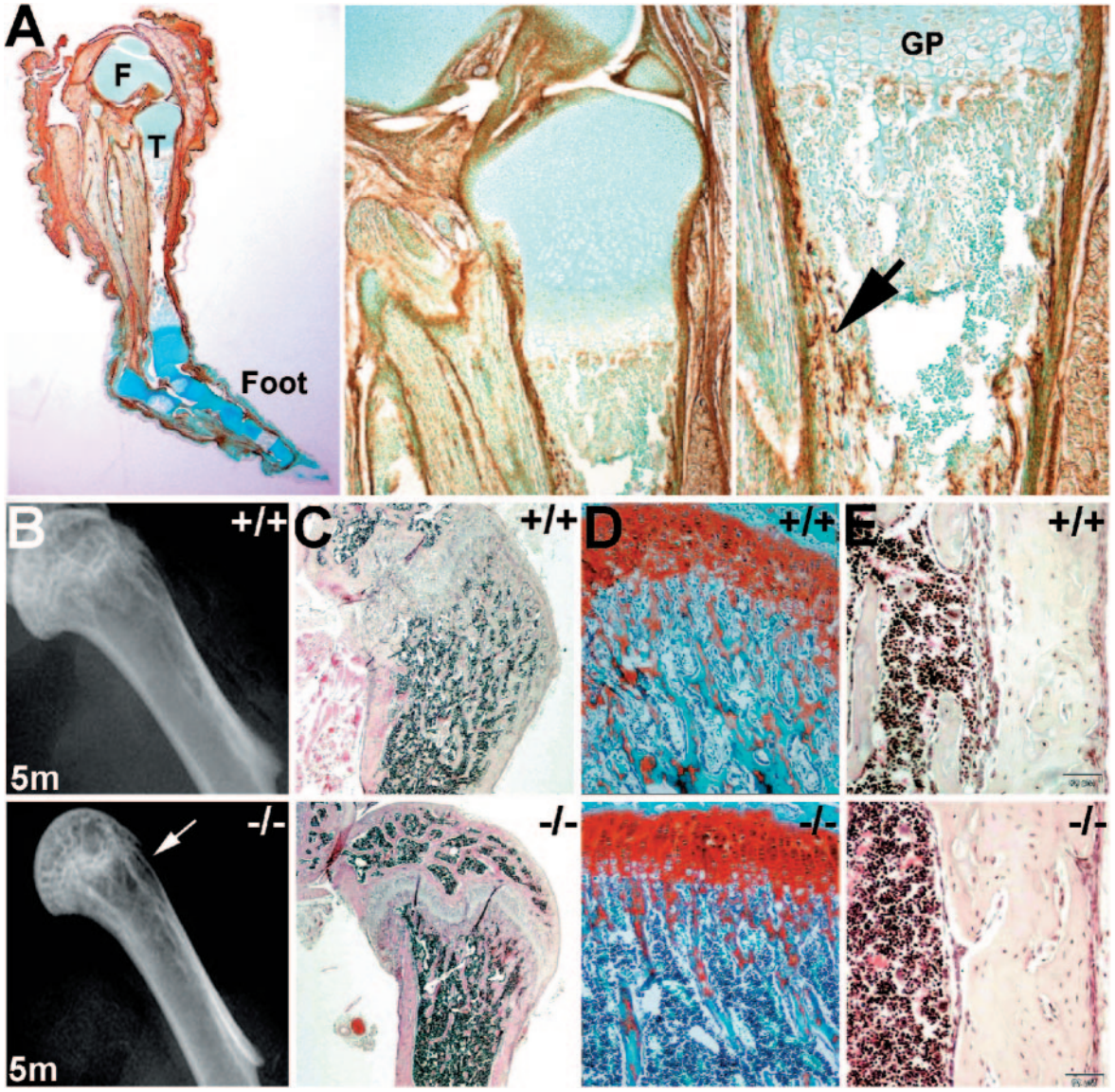

FIG. 4. Immunohistochemical analysis of periostin expression in wild-type limbs and analysis of long bone defects. (A) Wild-type 3-week-old decalcified hindlimb probed with periostin antibody and counterstained with methyl green. Note the particularly robust staining in periosteum around the distal femur (labeled "F" in panel A), tibia (labeled "T"), and foot bones as well as in the myotendinous junctions and underlying dermis of the skin. Middle panel: higher-power view of periostin in the proximal part of the tibial shaft epiphyses and synovial joint. Right panel: detailed view of epiphyseal growth plate (GP) region illustrating periostin localization within both the outer periosteum and inner endosteum and in cancellous bone in the mid-shaft region of the tibia (indicated by arrow). (B) Radiographic images of wild-type and null 5-month-old femur heads detect a lack of cancellous bony trabecula network in the null femur only (indicated by arrow). (C to E) Representative sections from decalcified 5-month-old wild-type (upper panels) and null (lower panels) femurs stained with H&E (C and E). Safranin-O staining of metaphysis (D) shows a significant reduction in bony trabeculae network in the nulls compared to that in wild-type sex-matched littermate controls. However, null bone marrow cellularity and volume appear unaffected.

required for muscle attachment (Fig. 5). As it is also well known that hypogonadal, hypothyroid, and pituitary-deficient mice exhibit postnatal growth deficiency, we examined *peri*^{lacZ} and periostin antibody expression in these tissues. Periostin was not expressed in the gonads, thyroid glands, or pituitaries. These organs all had normal histology (data not shown), suggesting that growth retardation is unlikely to be due to lack of growth hormones or to defects in the organs that secrete them.

***periostin* null females are infertile.** As both viable *peri*^{lacZ} null male and female adult mice were obtained, we examined their reproductive capabilities. Significantly, while the growth-retarded male nulls were fertile, the runted *peri*^{lacZ} null females were unable to become pregnant (even with wild-type males proven to be fertile). Histologically, the ovary, oviduct, and uterus all looked normal but were proportionally undersized. The *peri*^{lacZ} null females did get plugged (although irregularly), and the uterus could undergo a proliferative phase, but the vaginal plug persisted abnormally for up to 3 days (n = 16 mice). When the uteruses of *peri*^{lacZ} null female mice were harvested 6 to 10 days after plug detection and sectioned, we

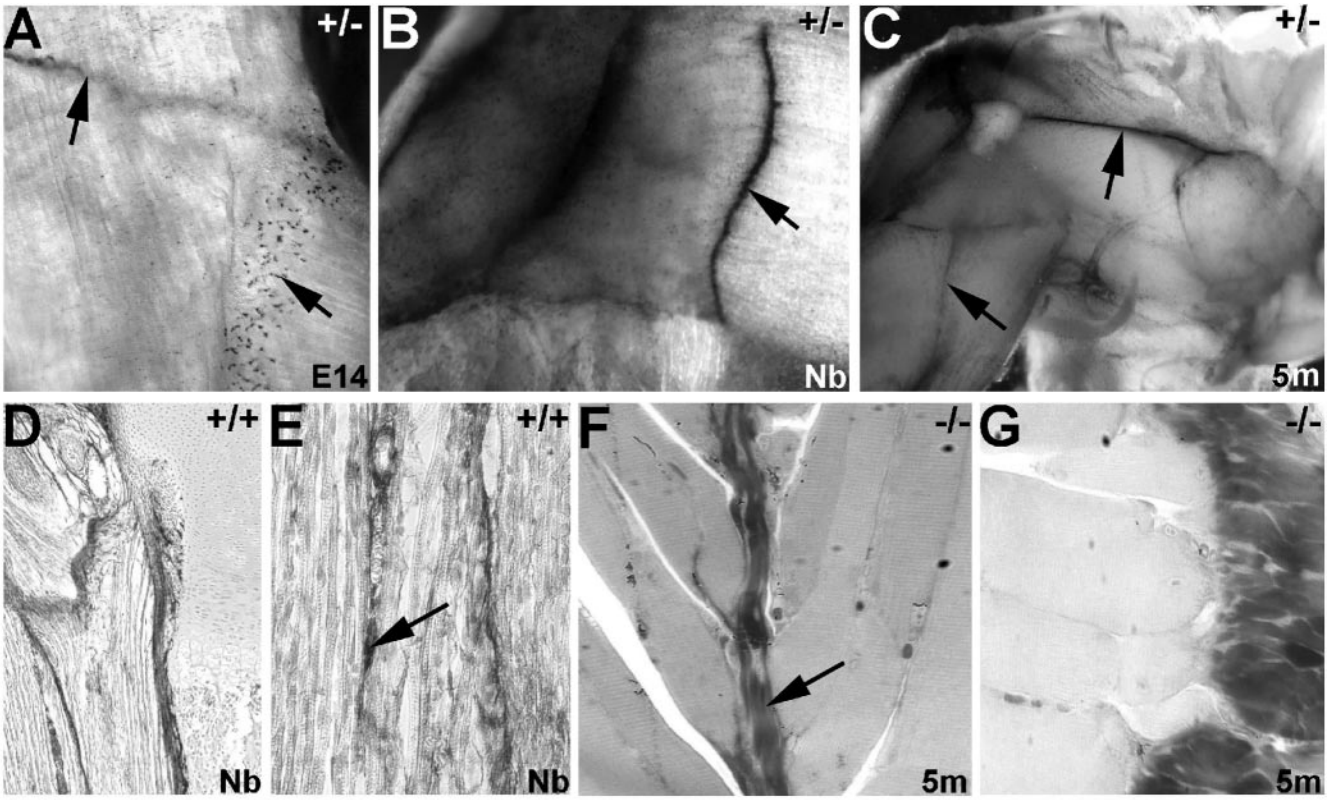

FIG. 5. $peri^{lacZ}$ nulls have normal myotendinous junctions. (A to C) *lacZ* staining of hindlimb musculature from $peri^{lacZ}$ +/− E14 (A), newborn (Nb) (B), and 5-month-old (5m) (C) mice. Note that $peri^{lacZ}$ is strongly expressed throughout myoseptal morphogenesis and that expression remains robust in adult life. (A) *periostin* reporter *lacZ* expression is present both in the large tendinous myoseptum that attaches fasciculus muscle bundles to each other (upper left arrow) and in smaller isolated muscle attachment sites (lower right arrow). (B and C) Once formed, the intramuscular tendons continue to express *lacZ* reporter expression. The arrow in panel B points to the myotendinous junction, as do arrows in panel C. (D and E) Immunohistochemical analysis revealed that periostin protein is present at similar levels both in the myotendinous junctions and in individual muscle attachment sites both at the intersections of muscles and in the supporting endomysium between individual muscle fibers (arrow in panel E). Additionally, periostin is robustly expressed in the periosteum at the ends of the skeletal muscle, where it directly attaches to the bone. (F and G) Ultrathin 1-μm sections of null intramuscular tendons (arrow in panel F) and myofibrils abutting the periosteum (G).

failed to detect any implantation sites or embryos. Additionally, when E2 to 3 oviducts of plugged null mice were sectioned, both two-cell and four-cell zygotes could be found (Fig. 6B). To gain further insight into the infertility, we induced superovulation with exogenous gonadotropins in immature +/+ mice and $peri^{lacZ}$ nulls to determine oocyte production. The superovulated +/+ mouse and $peri^{lacZ}$ null ovaries were similarly enlarged, and the numbers of primordial primary and antral follicles as well as of corpora lutea were proportionally equivalent (not shown), suggesting that hormonal response and ovarian folliculogenesis is intact. To determine whether the infertility and plug anomalies involve an abnormal estrous cycle, vaginal smear samples were taken daily from +/+ mice and $peri^{lacZ}$ nulls at 10 weeks of age for 1 month ($n = 6$ of each genotype). We found that the $peri^{lacZ}$ null mice failed to cycle (Fig. 6D), while the wild-type mice reached metestrus approximately every 7 days (Fig. 6C). Thus, the lack of normal estrus cycling may contribute to the infertility. Note that the mice were group housed, and it is known that group-housed mice have longer estrous cycles than individually housed mice (32).

$peri^{lacZ}$ nulls exhibit an early-onset periodontal disease-like phenotype. The PDL, situated between the cementum covering the root of the tooth and the bone forming the socket wall, contains at least two lineages of fibroblasts: common connective tissue fibroblasts and osteoblast-like fibroblasts (20). The PDL not only connects the tooth to the jaw bone but also supports the tooth in the socket and absorbs loads imposed on the tooth, thus protecting the tooth, especially at the root apex. Previous immunohistochemistry studies revealed high levels of periostin expression in the PDL, indicating that the periostin protein is present in the extracellular matrix and is possibly secreted from periodontal fibroblasts (10, 14). It was later found that the *periostin* mRNA-expressing cells are mainly fibroblastic cells in the PDL and osteoblastic cells on the alveolar bone surfaces (30). In addition, previous studies have reported that without tooth movement, the expression of *periostin* mRNA is uniformly observed in the PDL. However, *periostin* mRNA has been found to be up-regulated more in the pressure sites than in the tension sites after mechanical stress during experimental tooth movement (30).

To study the effects of loss of periostin on craniofacial mor-

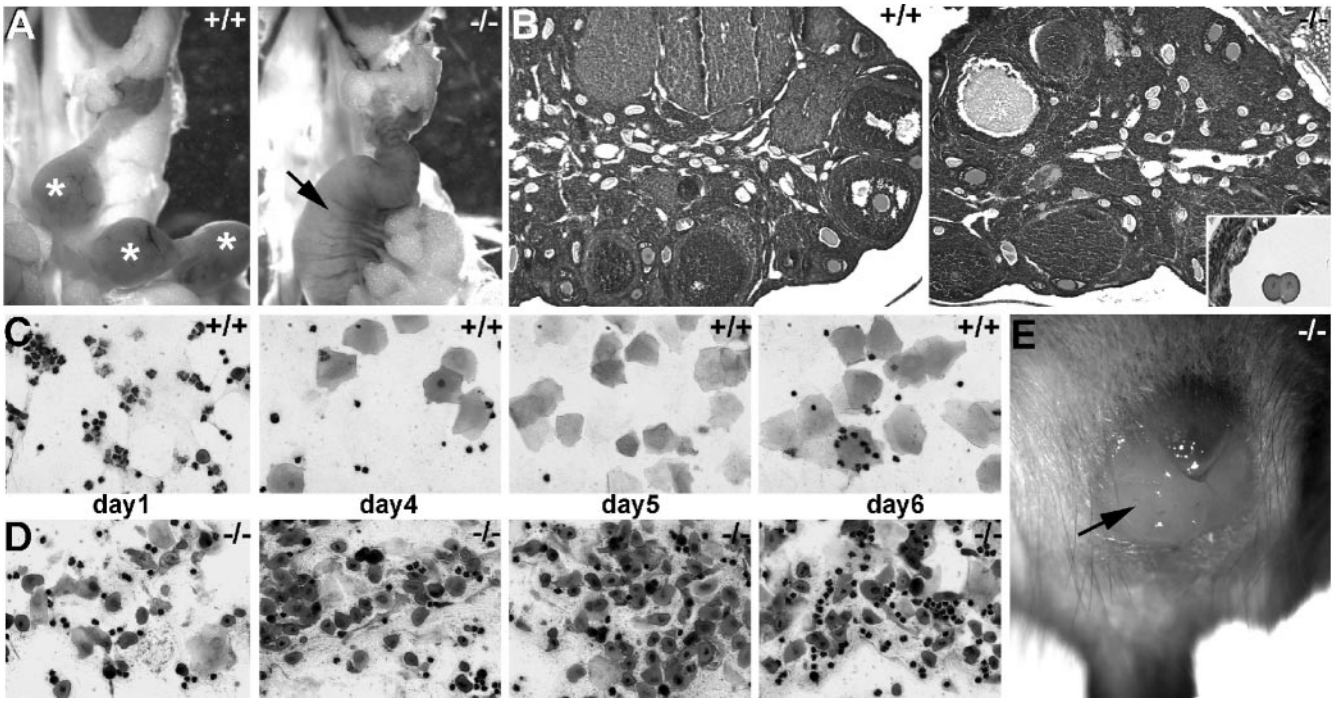

FIG. 6. Comparison of wild-type and *peri*^{lacZ} null female reproductive capabilities. (A) The genital tracts of 10-week-old female +/+ and −/− mice that had been plugged by fertile +/+ males. Note that the wild-type uterus has several individual E6.5 decidual swellings (indicated by ∗), while the null uteruses had undergone a proliferative response and are uniformly enlarged and highly vascularized (arrow). However, histological analysis revealed that only the wild-type uterus had implanted E6.5 embryos present. (B) Ovaries of 8 week-old +/− and −/− females were histologically similar (relative numbers of primordial, primary, and antral follicles as well as of corpora lutea were similar), although the null ovaries were proportionally smaller. Sectioning of the null oviducts revealed that two-cell null embryos were present (inset in B). (C and D) Vaginal smear samples taken during littermate estrous cycles revealed that while the wild-type mice had normal cycles, the nulls failed to cycle. (C) The wild-type mice had the normal 2- to 3-day diestrus (evidenced by presence of leukocytes almost exclusively) followed by rapid preestrus (equal numbers of leukocytes and nucleated epithelial cells), estrus (large transparent squamous epithelial cells), and postestrus (equal numbers of leukocytes and transparent squamous folded epithelial cells). (D) However, the null smear samples failed to reveal any recognizable phases of the menstrual cycle and appear to reflect a continuous postestrus/shedding stage. (E) Null vaginal copulation plugs abnormally persisted for up to 3 days (arrow), while wild-type plugs usually fell out within 12 h (n = 16 mice).

phogenesis, we confirmed that periostin is highly expressed in the wild-type PDL but absent in the nulls (Fig. 2B). Spatiotemporal analysis of the heterozygous *peri*^{lacZ} expression patterns throughout craniofacial development revealed that, like endogenous mRNA expression (14), high-level *lacZ* expression is present. Specifically, *peri*^{lacZ} is asymmetrically expressed in the lingual/palatal and buccal sides during the early epithelial-mesenchymal interactions. *peri*^{lacZ} is also present in dental papilla cells and in the transdifferentiating odontoblasts during the bell- and hard-tissue-formation stages of tooth development. Immunohistochemistry confirmed the localization, while Western blotting indicated that periostin protein is very stable, since levels remained high in the wild-type adults (data not shown).

At birth, the *peri*^{lacZ} null mice (n = 10) appear to have normal developing teeth and periodontia (Fig. 7A). However, at 4 weeks the fully erupted molars in the null mice display widening of the PDL, and the roots show signs of resorption. By the time the null mice reach the age of 3 months (n = 13), their periodontium appears dramatically affected, with distinct radiographic signs of alveolar bone destruction and external root resorption (Fig. 7B). Histologically, the periodontal defects are clearly evident, and a significant increase in osteoclast activity is seen in the periodontium of null mice, as shown by TRAP staining (Fig. 7C, D, and E).

Histological analysis of the PDL revealed a dramatic level of inflammatory infiltrate in the null mice (Fig. 7F). Interestingly, the inflammatory response cellular population is composed mainly of neutrophils, with fewer lymphocytes and plasma cells present (Fig. 7G). Overall, the inflammatory response appears to lead the PDL to undergo local conversion to granulation tissue. In fact, collagen III immunostaining supports this suggestion by showing increased signaling in the null mice that localizes within areas of the root and alveolar bone surface, which appear to be undergoing a repair attempt (Fig. 7H). Since collagen III is the primary component of early granulation tissue and has been associated with wound healing, this increase may represent the formation of scar tissue (26). We speculate that the nature of the stimulus that triggers the initial inflammatory response is traumatic. These continuous traumatic events might start with the eruption and consequent establishment of an occlusal relation between the mandibular and maxillary teeth.

Radiographic and histological evaluation of the dental and periodontal status of the *periostin* null mice led us to define this condition as a rapidly progressive periodontitis-like disorder;

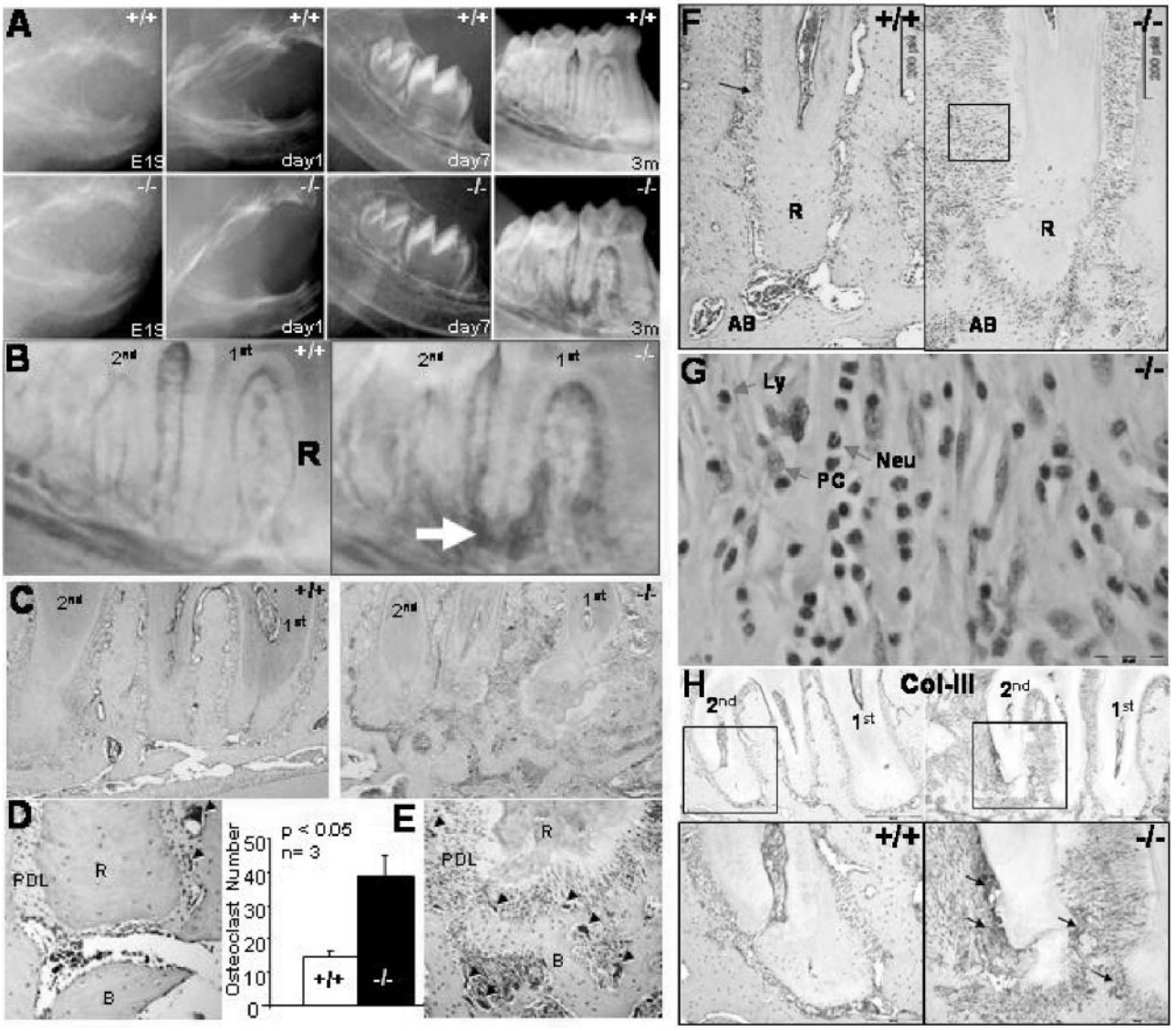

FIG. 7. Alveolar bone and PDL phenotype. (A) Wild-type and *peri*^{lacZ} null radiographic images from E19 to 3 months showing the formation of dental alveolar defects at 3 months. (B) Detailed radiographic images of the wild-type and null periodontia display bone resorption in the *peri*^{lacZ} null (arrow) but not in the wild type. (C) Histological analysis confirms loss of mutant alveolar bone and root reabsorption. (D) Tartrate-resistant acid phosphatase staining (black arrows) indicates an increase in osteoclast activity in the *periostin* null periodontium. (E) An almost threefold increase was detected in the *periostin* null mice after analyzing three different 3-month mandibular samples. (F) Adult 3-month second molar mesial root H&E-stained sections showing an increase in inflammatory infiltrate in the periodontal ligament of the *periostin* null mice. R, root; AB, alveolar bone. (G) The inflammatory response in the *peri*^{lacZ} null PDL is composed of numerous neutrophils (Neu), lymphocytes (Ly), and plasma cells (PC). (H) Collagen III (Col-III) immunostaining depicted areas of increased signaling on the surface of the 3-month-old *periostin* null molar root and alveolar bone.

its early appearance and apparent predisposition due to a structurally unstable PDL points out the requirement for periostin protein in the establishment of a biochemically stable PDL. In addition, foreign particles, such as hair shafts, can be observed in the *peri*^{lacZ} null PDL. These observations suggest that the *peri*^{lacZ} null PDL fails to establish a biological barrier between the oral cavity and the periodontium. Whether this is due to the loss of the PDL's mechanical properties due to the lack of *periostin* or is a secondary effect due to the dramatic vertical bone loss is currently unknown.

***peri*^{lacZ} nulls have a severe incisor enamel defect.** The distribution of cell adhesion molecules and substrate adhesion molecules as potential regulatory factors in tooth development has been a subject of increasing interest. Periostin, a cell adhesion molecule that has been found to be preferentially expressed in the PDL, was reported to be ligand for αvβ3 and αvβ5 integrins and to promote αvβ3 and αvβ5 integrin-dependent cell adhesion and enhance cell motility (8). Interestingly, integrins appeared to be involved in the interaction of PDL and gingival fibroblasts with the enamel matrix protein (29).

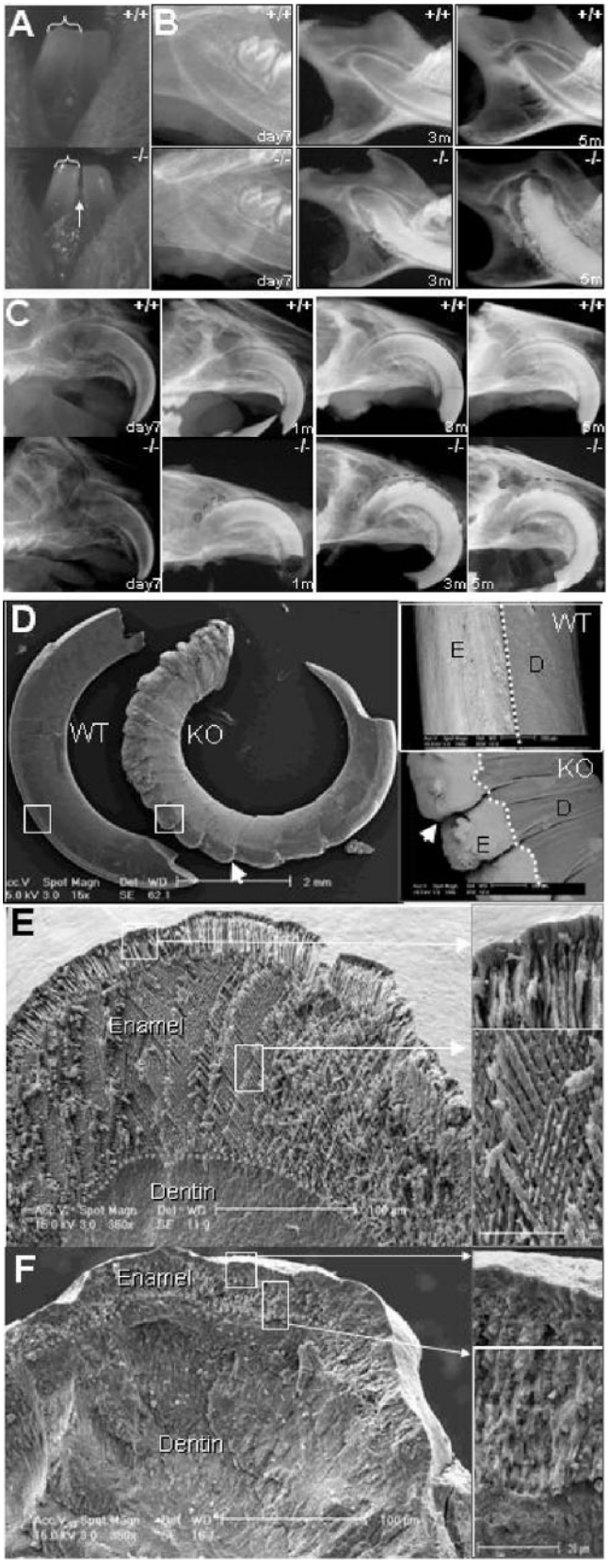

FIG. 8. Incisor enamel defects in *peri*^{lacZ} null mice. (A) Incisor phenotype. A mandibular facial view of young 3-week-old incisor teeth from the wild type shows the typical translucent appearance of enamel that is reflected through the enamel layer on its surface. The dentin has a yellowish color. In contrast, the null incisors appear thinner and present a mesial interproximal gap (arrow), and their enamel layer appears less translucent, which gives a mild opacity to its surface. Brackets indicate reduced incisor width. (B) Radiographic view of the mandibular periapical region shows the progression of the enamel defect from day 7 to 5 months of age. (C) Radiographic view of the maxillary incisor at day 7, where no apparent defect is detectable in the *peri*^{lacZ} null mice, and of that of the 5-month-old (5m) *peri*^{lacZ} null mice, which displays a complete deformation of the enamel surface that affects the incisor from the apex to the incisal edge. Notice the anterior progression of the defect that is initially detected at 1 month. (D) Backscatter SEM images of 3-month-old maxillary incisors show clefting of the enamel surface in the *periostin* null incisors (indicated by arrows). E, enamel surface; D, dentin surface; WT, wild type; KO, knockout. (E) Coronal sections from the wild-type incisor show the typical enamel prism structure pattern. (F) In contrast to the wild type, the *peri*^{lacZ} null mice exhibit an abnormally thin enamel layer with an apparent amorphous and irregular prism pattern. For panels D, E, and F, boxed regions in left panels are shown at higher magnification to the right.

Unlike those of other mammals, rodent incisors are continuously erupting throughout adult life, with a highly active enamel-producing organ positioned in the future facial incisor surface. This unique rodent characteristic allows us to evaluate the effects that periostin has in the developing incisor under conditions of occlusal mechanical stress. Radiographic evaluation of the *peri*^{lacZ} null mice ($n = 18$) revealed a severe incisor enamel defect that progressively deformed the entire facial enamel surface of the mandibular and maxillary incisors (Fig. 8B and C). Although radiographically there appears to be no difference between the *peri*^{lacZ} null mouse incisor and the control incisor during the first 3.5 weeks and prior to weaning, the initial clinical gross manifestation in the null incisor enamel resembles a hypoplastic-like condition characterized by a less translucent enamel surface and by a decrease in the incisor's mesial-distal area, which leads to the presence of a mandibular incisor interproximal space in the *periostin* null mice (Fig. 8A). By 5 months, the enamel defects have worsened, and a highly radiopaque deformed surface that extends from the apex towards the incisal edge can be clearly detected radiographically (Fig. 8B and C). Further analysis of the incisors by use of BSEM highlights the abnormally worn incisal edge and the deformed and cleft enamel surface on the *peri*^{lacZ} null incisors (Fig. 8D). Analysis of the cross-sectional view of the enamel and dentin structure using secondary SEM shows a well-defined enamel prism organization in the wild type (Fig. 8). In contrast, the *peri*^{lacZ} nulls exhibit a much thinner enamel layer with an irregular and ill-defined pattern (Fig. 8F).

Histologically, the wild-type adult mice present a well-organized ameloblast layer composed of a polarized cylindrical simple epithelium. In contrast, the *peri*^{lacZ} nulls display a disorganized pseudostratified epithelial layer which appears to produce an amorphous matrix that covers the dentin and is also present ectopically within this matrix-producing organ (Fig. 9A). Although the abnormal *peri*^{lacZ} null enamel epithelium has lost its normal ameloblast characteristics, it continues synthesizing amelogenin, an ameloblast-specific marker (Fig. 9B). TEM visualization of the ameloblast from *peri*^{lacZ} nulls shows clusters of epithelial cells containing secretion

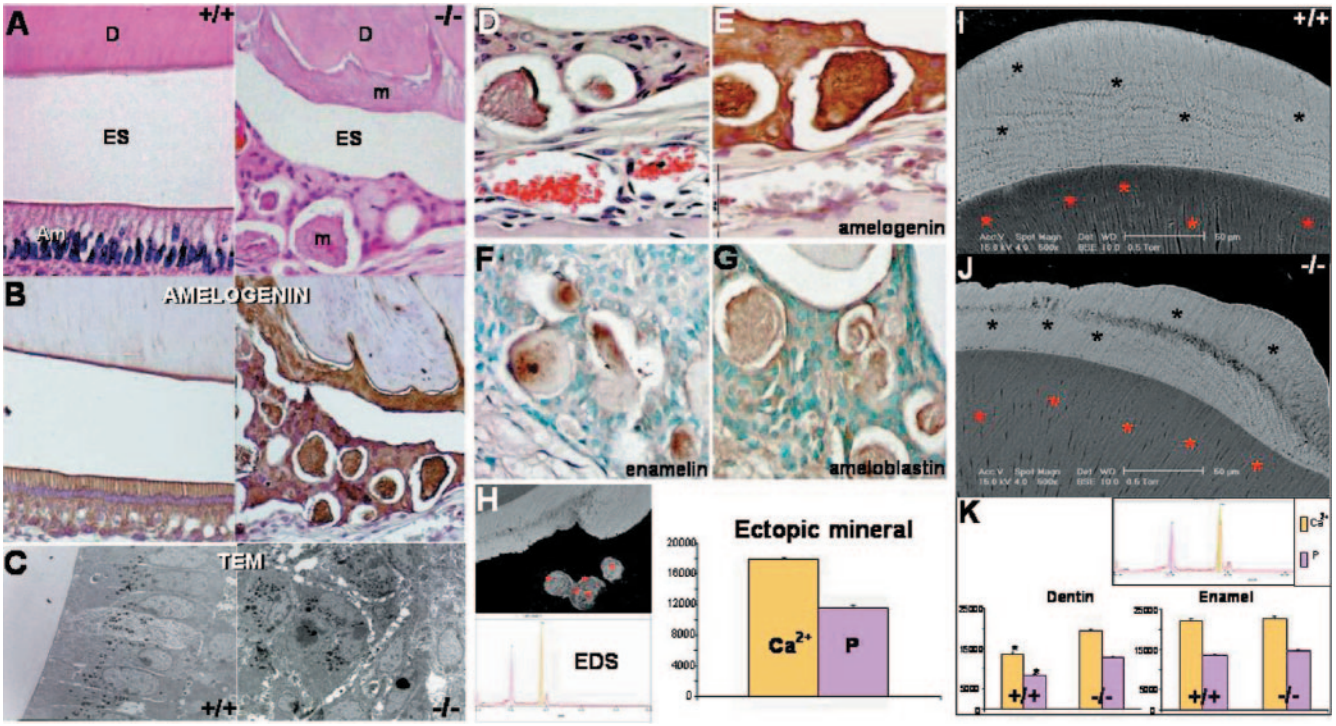

FIG. 9. Ameloblast defects in *peri*^{lacZ} nulls. (A) H&E-stained sections of the wild-type and *peri*^{lacZ} null mouse ameloblasts from the apical third of the mandibular incisor. Notice the normal polarized cylindrical epithelial layer formed in the wild type. In contrast, the *peri*^{lacZ} null mice show a completely distorted epithelium with a pseudostratified appearance. Notice the matrix within the enamel space that remains after decalcification and the isolated globular structures. D, dentin; Am, ameloblast; m, matrix; ES, enamel space. (B) Both the normal ameloblasts in the wild type and the pseudostratified layer and amorphous matrix in the null mice stain positive with a polyclonal antibody against amelogenin, which is an ameloblast-specific marker. (C) TEM allows the detection of normal formation of secretory granules within the clustered ameloblasts in the *peri*^{lacZ} null mice, as seen in the normal ameloblast layer (dark cytoplasmic granules). (D to G) Immunohistochemistry studies showed that the globular structures in the null ameloblastic epithelium were positive for amelogenin, enamelin, and ameloblastin. (H) In addition, these globular structures contain calcium and phosphate within the matrix, as shown by EDS. (I and J) BSEM cross-sectional images from plastic-embedded, polished samples highlight the enamel defects within the null matrix, shown as darker areas. In addition, the dentin in the null mice appears brighter, which indicates a high degree of mineralization compared with that in the wild type. Bars, 50 μm. (K) EDS readings from five different areas within the dentin matrix support the backscatter findings, indicating a significant increase in calcium and phosphate intensities in the *peri*^{lacZ} null dentin over those in the wild-type control. However, despite the described enamel defects, no significant difference in calcium and phosphate intensities within the enamel was detected using EDS.

granules, which are characteristic of functionally active ameloblast cells (Fig. 9C). We confirmed the presence of normal enamel proteins within the ectopic matrix structures by use of antibodies against amelogenin, enamelin, and ameloblastin (Fig. 9D to G). In addition, we detected calcium and phosphate within these ectopic structures by use of energy-dispersive X-ray spectroscopy (EDS) in plastic-embedded and highly polished specimens (Fig. 9H). The mineral intensities in these structures were similar to those in normal dentin. The same measurements were acquired for the *peri*^{lacZ} null enamel layer and dentin. Interestingly, the spectroscopy readings revealed no significant difference in calcium and phosphate intensities in the enamel matrix from the two groups; however, obvious structural defects were visible in the dentin matrix of the null mice (Fig. 9I and J). In addition, EDS measurements and backscatter images of dentin (Fig. 9I and J) indicate a hypermineralization of the *peri*^{lacZ} null mouse dentin which, together with the observed obliteration of the incisor canals, might be induced in an attempt to compensate for the presence of a structurally unstable enamel layer.

The fact that these ameloblast defects occur only postnatally (as the newborn and 2-week-old null ameloblast layer shows no defects and has an intact basement membrane) probably explains why we do not see any enamel incisor defects during the first 3 weeks. This suggests that when the teeth erupt and start undergoing constant mechanical stimulation during feeding, the lack of periostin affects the structural integrity of the already differentiated enamel-producing organ, and it is this perturbation that results in the abnormal deposition of the enamel matrix. In support of this are our observations that the molars show no signs of enamel or dentin anomalies within the crown, as these developed while the teeth are unerupted and thus were protected from any significant mechanical stresses. Similarly, analysis of both *amelogenin* knockout (7) and overexpressor (21) mutant mice that have a hypoplastic enamel lacking the normal prism structure supports the idea that alterations to the ECM can be reflected as defects in the structural organization of enamel. Thus, these data suggest that initial *peri*^{lacZ} null ameloblast-odontoblast interactions take place normally and that the basement membrane is intact in newborn nulls, but that postnatally there is a lack of enamel organ integrity.

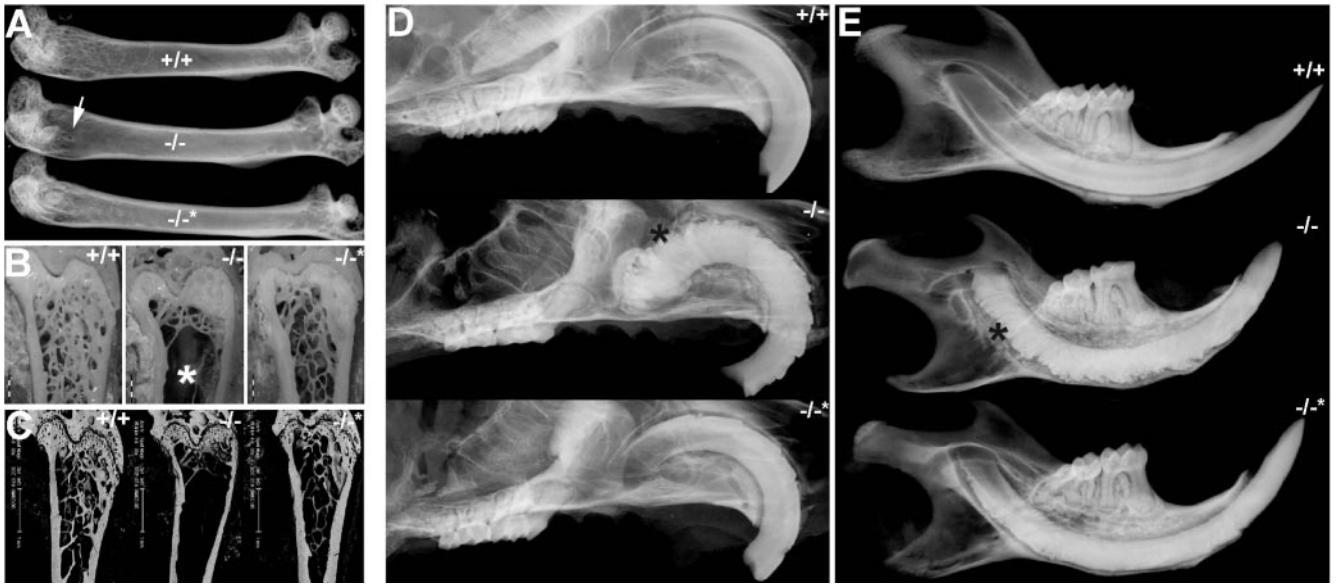

FIG. 10. Amelioration of skeleton and enamel defects in *peri*^{lacZ} nulls by changing diet. (A) Radiographic images of 6-month-old femurs either from wild-type and *peri*^{lacZ} null mice fed standard pellet chow (+/+ and −/−) or from *peri*^{lacZ} null littermate mice fed powdered soft chow (−/−*). Note that while the femur head from a null fed standard chow exhibited a reduced bony trabecula network (indicated by arrow), that of the null fed powdered chow appeared similar that of the wild-type littermate. (B and C) Visualization of femur head cancellous bony trabecula network sagittal sectional images from plastic-embedded polished samples (B) and via BSEM (C). Note that nulls fed powdered chow have grossly normal trabecular bone compared to null littermates fed standard chow. (D) Radiographic views of the maxillary incisor region show that only nulls fed standard chow exhibit complete deformation of the enamel surface that affects the incisor from the apex to the incisor edge (indicated by *), while the nulls fed powdered chow (−/−*) exhibit only mild clefting of the enamel surface. (E) Similarly, radiographic views of the mandible support the findings that the null enamel and incisor defects are somewhat prevented by feeding with soft rather than standard chow.

Feeding nulls powdered food rescues female infertility and ameliorates null skeleton, enamel, and dwarfism defects. Given the severely reduced postnatal body weight, undersized skeleton, female-only infertility, and craniofacial remodeling defects, we wondered which of these various defects were primary and which might have been secondary and due to malnourishment postweaning. Thus, in order to test whether any of these observed phenotypes were due to an inability to eat properly, age-matched homozygous null littermates were either placed on a soft powdered diet or maintained on standard pellet chow for 6 months following weaning ($n = 47$ nulls; 27 on powdered and 20 on regular chow). Significantly, decreasing mechanical stress via feeding soft chow tended to ameliorate the characteristic null incisor defects and grossly rescued the cancellous trabecular bony network within the long bones. Radiographic, histologic, and BSEM analysis of 6-month-old null femurs from mice fed powdered chow have grossly normal trabecular bone indistinguishable from that of wild types, which is in contrast to results for null littermates fed standard chow (Fig. 10A to C). Similarly, radiographic analysis of their craniofacial elements revealed that only *peri*^{lacZ} nulls fed standard chow exhibit complete deformation of the enamel surface, but that the nulls fed powdered chow exhibit only mild clefting of the enamel surface (Fig. 10D and E). Body weights (4-month-old standard-fed +/+ mice were 34.8 ± 1.40 g [$P < 0.005$]; standard-fed −/− mice were 21.0 ± 0.61 g [$P < 0.005$]; −/− mice fed powdered chow were 28.8 ± 0.75 g [$P < 0.005$]) and femur and tibial lengths (standard-fed +/+ and −/− mice fed powdered chow were similar in this regard, while standard-fed −/− long bones were ~11% reduced in length) of the nulls fed soft chow also improved. Most significantly, some of the female nulls fed powdered chow were capable of carrying and delivering pups following mating with both wild-type and null males, although with reduced fecundity compared to that of wild-type females fed the standard pellet diet (3.1 ± 0.6 litters per +/+ female versus 1.7 ± 0.5 litters per powder-fed −/− female over 12 weeks, but average litter sizes were similar: 8.0 ± 2.5 pups for +/+ females and 7.5 ± 3.1 pups for nulls). These results indicate that reduced mastication not only dramatically improves *peri*^{lacZ} null postnatal craniofacial maturation but also indirectly improves growth and fertility. Thus, despite the fact that periostin is transiently expressed in the uterine endometrial lining at the time of implantation and that periostin itself can be induced by progesterone (3), these data show that periostin itself is not required for mouse fertility but may be a useful marker in the investigation of the physiological events leading up to implantation in both normal and malnourished pregnancies. Furthermore, the amelioration of null skeleton and dwarfism defects suggests that the postnatal role of periostin within the periosteum may be redundant and certainly is not a major requirement during bone growth and maintenance. Further studies are under way to determine whether the loss of trabecular bone is due to abnormal remodeling secondary to reduced osteoblast numbers and function, perturbed osteoblast/osteoclast dynamics or lack of bone maintenance or is simply an endocrinological response to vitamin, nutrient, and/or mineral deficiency(ies). However, periostin may play an active role in repair of bone fractures, as the mature periosteum is also thought to house the osteoprogenitor cells that are responsible for bone repair. In support of this, periostin has

been shown to be a specific marker of preosteoblasts and could play an important role in periosteal callus formation during the early stage of fracture healing (19).

Periostin is required to cushion and mediate mechanical forces. Mechanical forces are known to have effects on bone formation, maintenance, and remodeling, and there is evidence that mechanical stresses induced by mastication can influence (both morphologically and molecularly) rodent craniofacial tissues as well (23, 24). By decreasing the mechanical stress during feeding, we have demonstrated that a periostin-expressing PDL is required to absorb and/or mediate the stresses placed on the teeth and their attachments to the jaw.

The above observations suggest that the null ameloblast cells are fully differentiated but are unable to maintain their usual ameloblast morphology as an intact single layer under stress. Lack of organization of the ameloblast layer has been previously linked to loss of an intact basement membrane and epithelial anchorage (33). Additionally, as ameloblasts become elongated upon differentiation, they could become more susceptible to mechanical forces during postnatal development. During the application of mechanical forces, positional information and cell-to-cell adhesions become critical prerequisites for the structural integrity of ameloblasts (2, 18). Given the profound ultrastructural and histological changes in the ameloblasts and enamel defects in the *peri*^{lacZ} null mice, we propose that the PDL plays an important role in supporting normal ameloblast function and maintenance of the enamel matrix, and that periostin, an adhesive molecule, may be required for this role. This requirement appears to be necessary only under particular circumstances, specifically when the periodontium is sustaining significant amounts of mechanical stress, such as in the case of occlusal function during mastication. The severities of these *peri*^{lacZ} null enamel defects are underscored by the fact that enamel rarely undergoes catastrophic failure despite a lifetime of repeated loading, in a wet, acidic, and bacterium-laden environment (22). Thus, the continued high expression of both *periostin* mRNA and protein in the adult PDL ECM may indicate that *periostin* maintains the PDL as a nonmineralized barrier tissue and as a renewable source of cells required for the regeneration of the alveolar bone and root cementum. Further studies are under way to determine the potential role of *periostin* in the alveolar bone regeneration process and to determine whether it is also affected during the pathogenesis of periodontal diseases.

Conclusions. Combined, these data suggest that *periostin* may be required in utero for events that manifest themselves only in postnatal life, but that it is not essential for in utero survival. These data firmly establish that the postnatal maintenance role of *periostin* is vital. Specifically, they demonstrate that *periostin* is required for the maintenance of the postnatal PDL and that a lack of *periostin* leads to traumatic dental-alveolar stimuli and an increased susceptibility for bacterial invasion, which leads to a severe inflammatory and immune response. Future studies are required to determine which specific proinflammatory cytokines (12) that stimulate the formation and activation of osteoclasts that ultimately leads to the observed jaw bone loss and external root resorption are induced. Furthermore, the rodent incisor's lifespan-lasting enamel organ defects observed in the *peri*^{lacZ} null mice led us to propose that *periostin* is also required for the integrity, absorption of mechanical stresses, and anchorage of the ameloblast lineage and that a lack of *periostin* leads to defects in ameloblast morphology and function that result in the secretion of inappropriate amorphous matrix and abnormal enamel structure, ultimately resulting in enhanced tooth wear.

ACKNOWLEDGMENTS

These studies were supported, in part, by National Institutes of Health grants HL33756, HL60714 (S.J.C), and DE13480 (J.Q.F) and by NIDCR training grant T32DE07294 (H.R).

REFERENCES

1. **Bao, S., G. Ouyang, X. Bai, Z. Huang, C. Ma, M. Liu, R. Shao, R. M. Anderson, J. N. Rich, and X. F. Wang.** 2004. Periostin potently promotes metastatic growth of colon cancer by augmenting cell survival via the Akt/PKB pathway. Cancer Cell **5:**329–339.
2. **Bei, M., S. Stowell, and R. Maas.** 2004. Msx2 controls ameloblast terminal differentiation. Dev. Dyn. **231:**758–765.
3. **Cheon, Y. P., Q. Li, X. Xu, F. DeMayo, I. Bagchi, and M. K. Bagchi.** 2002. A genomic approach to identify novel progesterone receptor regulated pathways in the uterus during implantation. Mol. Endocrinol. **16:**2853–2871.
4. **Conway, S. J., D. Henderson, and A. Copp.** 1997. Pax3 is required for cardiac neural crest migration in the mouse: evidence from the splotch (Sp2H) mutant. Development **124:**505–514.
5. **Dickman, E. D., R. Rogers, and S. J. Conway.** 1999. Abnormal skeletogenesis occurs coincident with increased apoptosis in the Splotch (Sp2H) mutant: putative roles for Pax3 and PDGFRalpha in rib patterning. Anat. Rec. **255:**353–361.
6. **Ferguson, J. W., M. Mikesh, E. Wheeler, and R. G. LeBaron.** 2003. Developmental expression patterns of Beta-ig (betaIG-H3) and its function as a cell adhesion protein. Mech. Dev. **120:**851–864.
7. **Gibson, C. W., Z. Yuan, B. Hall, G. Longenecker, E. Chen, T. Thyagarajan, T. Sreenath, J. T. Wright, S. Decker, R. Piddington, G. Harrison, and A. B. Kulkarni.** 2001. Amelogenin-deficient mice display an amelogenesis imperfecta phenotype. J. Biol. Chem. **276:**31871–31875.
8. **Gillan, L., D. Matei, D. A. Fishman, C. Gerbin, B. Y. Karlan, and D. D. Chang.** 2002. Periostin secreted by epithelial ovarian carcinoma is a ligand for alpha(V)beta(3) and alpha(V)beta(5) integrins and promotes cell motility. Cancer Res. **62:**5358–5364.
9. **Harris, S. E., M. Sabatini, M. Harris, J. Q. Feng, J. Wozney, and G. R. Mundy.** 1994. Expression of bone morphogenetic protein messenger RNA in prolonged cultures of fetal rat calvarial cells. J. Bone Miner. Res. **9:**389–394.
10. **Horiuchi, K., N. Amizuka, S. Takeshita, H. Takamatsu, M. Katsuura, H. Ozawa, Y. Toyama, L. F. Bonewald, and A. Kudo.** 1999. Identification and characterization of a novel protein, periostin, with restricted expression to periosteum and periodontal ligament and increased expression by transforming growth factor beta. J. Bone Miner. Res. **14:**1239–1249.
11. **Katsuragi, N., R. Morishita, N. Nakamura, T. Ochiai, Y. Taniyama, Y. Hasegawa, K. Kawashima, Y. Kaneda, T. Ogihara, and K. Sugimura.** 2004. Periostin as a novel factor responsible for ventricular dilation. Circulation **1101:**1806–1813.
12. **Kawashima, N., and P. Stashenko.** 1999. Expression of bone-resorptive and regulatory cytokines in murine periapical inflammation. Arch. Oral Biol. **44:**55–66.
13. **Koushik, S., J. Wang, R. Rogers, D. Miskophidis, N. Lambert, T. Creazzo, and S. J. Conway.** 2001. Targeted inactivation of the sodium-calcium exchanger (Ncx1) results in the lack of a heartbeat and abnormal myofibrillar organization. FASEB J. **15:**1209–1211.
14. **Kruzynska-Frejtag, A., J. Wang, M. Maeda, R. Rogers, E. Krug, S. Hoffman, R. Markwald, and S. J. Conway.** 2004. Periostin is expressed within the developing teeth at the sites of epithelial-mesenchymal interaction. Dev. Dyn. **229:**857–868.
15. **Kruzynska-Frejtag, A., M. Machnicki, R. Rogers, R. Markwald, and S. J. Conway.** 2001. Periostin (an osteoblast-specific factor) is expressed within the embryonic mouse heart during valve formation. Mech. Dev. **103:**183–188.
16. **Kudo, H., N. Amizuka, K. Araki, K. Inohaya, and A. Kudo.** 2004. Zebrafish periostin is required for the adhesion of muscle fiber bundles to the myoseptum and for the differentiation of muscle fibers. Dev. Biol. **267:**473–487.
17. **Lindsley, A., W. Li, J. Wang, N. Maeda, R. Rogers, and S. J. Conway.** 2005. Comparison of the four mouse fasciclin-containing genes expression patterns during valvuloseptal morphogenesis. Gene Expr. Patterns **5:**593–600.
18. **Meyer, J. M., J. V. Ruch, M. Kubler, C. Kupferle, and H. Lesot.** 1995. Cultured incisors display major modifications in basal lamina deposition without further effect on odontoblast differentiation. Cell Tissue Res. **279:** 135–147.
19. **Nakazawa, T., A. Nakajima, N. Seki, A. Okawa, M. Kato, H. Moriya, N. Amizuka, T. A. Einhorn, and M. Yamazaki.** 2004. Gene expression of periostin in the early stage of fracture healing detected by cDNA microarray analysis. J. Orthop. Res. **22:**520–525.

20. **Nanci, A.** 2003. Ten Cate's oral histology: development, structure, and function, 6th ed. Mosby, St. Louis, Mo.
21. **Paine, M. L., H. J. Wang, W. Luo, P. H. Krebsbach, and M. L. Snead.** 2003. A transgenic animal model resembling amelogenesis imperfecta related to ameloblastin overexpression. J. Biol. Chem. **278:**19447–19452.
22. **Paine, M. L., S. N. White, W. Luo, H. Fong, M. Sarikaya, and M. L. Snead.** 2001. Regulated gene expression dictates enamel structure and tooth function. Matrix Biol. **20:**273–292.
23. **Salo, L. A., J. Hoyland, S. Ayad, C. Kielty, A. Freemont, P. Pirttiniemi, T. Kantomaa, M. E. Grant, and J. T. Thomas.** 1996. The expression of types X and VI collagen and fibrillin in rat mandibular condylar cartilage. Response to mastication forces. Acta Odontol. Scand. **54:**295–302.
24. **Sasaguri, K., H. Jiang, and J. Chen.** 1998. The effect of altered functional forces on the expression of bone-matrix proteins in developing mouse mandibular condyle. Arch. Oral Biol. **43:**83–92.
25. **Sasaki, H., Y. Sato, S. Kondo, I. Fukai, M. Kiriyama, Y. Yamakawa, and Y. Fuji.** 2002. Expression of the periostin mRNA level in neuroblastoma. J. Pediatr. Surg. **37:**1293–1297.
26. **Sodek, J., D. Brunette, J. Feng, J. Heersche, H. Limeback, A. H. Melcher, and B. Ng.** 1977. Collagen synthesis is a major component of protein synthesis in the periodontal ligament in various species. Arch. Oral Biol. **22:** 647–653.
27. **Stanton, L. W., L. Garrard, D. Damm, B. Garrick, A. Lam, A. M. Kapoun, Q. Zheng, A. Protter, G. Schreiner, and R. T. White.** 2000. Altered patterns of gene expression in response to myocardial infarction. Circ. Res. **86:**939–945.
28. **Takeshita, S., R. Kikuno, K. Tezuka, and E. Amann.** 1993. Osteoblast-specific factor 2: cloning of a putative bone adhesion protein with homology with the insect protein fasciclin I. Biochem. J. **294:**271–278.
29. **van der Pauw, M. T., V. Everts, and W. Beertsen.** 2002. Expression of integrins by human periodontal ligament and gingival fibroblasts and their involvement in fibroblast adhesion to enamel matrix-derived proteins. J. Periodontal Res. **37:**317–323.
30. **Wilde, J., M. Yokozeki, K. Terai, A. Kudo, and K. Moriyama.** 2003. The divergent expression of periostin mRNA in the periodontal ligament during experimental tooth movement. Cell Tissue Res. **312:**345–351.
31. **Ye, L., M. MacDougall, S. Zhang, Y. Xie, J. Zhang, Z. Li, Y. Lu, Y. Mishina, and J. Q. Feng.** 2004. Deletion of dentin matrix protein-1 leads to a partial failure of maturation of predentin into dentin, hypomineralization, and expanded cavities of pulp and root canal during postnatal tooth development. J. Biol. Chem. **279:**19141–19148.
32. **Zaczek, D., J. Hammond, L. Suen, S. Wandji, D. Service, A. Bartke, V. Chandrashekar, K. Coschigano, and J. Kopchick.** 2002. Impact of growth hormone resistance on female reproductive function: new insights from growth hormone receptor knockout mice. Biol. Reprod. **67:**1115–1124.
33. **Zhou, H. M., A. Nichols, A. Wohlwend, I. Bolon, and J. D. Vassalli.** 1999. Extracellular proteolysis alters tooth development in transgenic mice expressing urokinase-type plasminogen activator in the enamel organ. Development **126:**903–912.